Mechanism and Machine Theory 44 (2009) 1701–1712

Contents lists available at ScienceDirect

Mechanism and Machine Theory

journal homepage: www.elsevier.com/locate/mechmt

Mathematical model and worm wheel tooth working surfaces of the ZN-type hourglass worm gear set

Kuan-Yu Chen [a], Chung-Biau Tsay [b,*]

[a] Department of Mechanical Engineering, National Chiao Tung University, Hsinchu 30010, Taiwan, ROC
[b] Department of Mechanical Engineering, Minghsin University of Science and Technology, No. 1, Hsin-Hsin Road, Hsinchu 30401, Taiwan, ROC

ARTICLE INFO

Article history:
Received 18 September 2008
Received in revised form 30 January 2009
Accepted 10 February 2009
Available online 21 March 2009

Keywords:
ZN-type hourglass worm gear set
Worm-type hob cutter
Boundary line
Contact line
Tooth working surface

ABSTRACT

In this study, the hourglass worm gear set is composed of a ZN-type hourglass worm generated by straight-edged blade cutters and a ZN-type hourglass worm wheel generated by worm-type hourglass hob cutters. Mathematical model of the ZN-type hourglass worm gear set is derived based on its generation mechanism and the theory of gearing. According to the developed mathematical model of the gear set, computer graphs of the ZN-type hourglass worm and worm wheel are presented. The tooth working surface, boundary lines and contact lines of the ZN-type hourglass worm gear set under different lead angles, pressure angles and modules are investigated and compared with those of the ZA-type hourglass worm gear set.

1. Introduction

Characteristics and contact nature of the worm gear set have been investigated by many researchers. Due to their efforts, the efficiency and working life time of worm gear sets have been improved substantially. Compared with the conventional worm gear drive, the hourglass worm gear drive provides a higher contact ratio. Gear drives with a higher contact ratio may increase the absorbability of impact loads subjected to machines. Maki and Sakai [1] developed a new type of hourglass worm gearing that its tooth surfaces can be ground precisely. Ishida [2] investigated a new plane toothed worm wheel and its enveloping hourglass worm. Maki and Sakai [3] also studied the hourglass worm gearing with contact slide-roll ratio. Winter and Wilkesmann [4] proposed a calculation method of obtaining more precise worm surfaces. Simon [5,6] investigated the manufacturing of a high precision hob for worm surface generations. Simon [7,8] also proposed a ground double-enveloping worm gear drive. The gear tooth surface of the ground worm gearing is smooth, and it is shaped by a flying tool whose cutting edge is identical to the profile of the entering edge of worms. Simon [9,10] also studied the double-enveloping worm gearing with a better elastohydrodynamic load carrying capacity and lower power losses. Gunbara et al. [11] brought applications to the gear design by using two kinds of hourglass worm gears with larger lead angles. Fang and Tsay [12] derived mathematical model of the ZN-type worm gear set based on the hobbing mechanism and hob cutter's parameters. Janninck [13] proposed a method for predicting the initial contact pattern and showed their results by applying a surface separation topological diagram over the entire worm wheel surface. Litvin [14] and Litvin and Fuentes [15] developed the mathematical model of the ZA-type hourglass worm gear set. Shi et al. [16] studied the contact deformation of a

* Corresponding author. Tel.: +886 919 976 928.
E-mail address: cbtsay@mail.nctu.edu.tw (C.-B. Tsay).

0094-114X/$ - see front matter © 2009 Elsevier Ltd. All rights reserved.
doi:10.1016/j.mechmachtheory.2009.02.003

double-enveloping worm gearing that the shift of contact zone and load share among the meshing tooth-pairs were analyzed by using the three-dimensional contact FEM.

In this study, a ZN-type hourglass worm gear set is investigated. The ZN-type hourglass worm is cut by a straight-edged cutting blade, and the ZN-type hourglass worm wheel is produced by a worm-type hourglass hob cutter which is identical to the ZN-type hourglass worm. The mathematical model of the ZN-type hourglass worm gear set is developed according to the theory of gearing and the gear generation mechanism. The bearing contacts of the generated conjugate hourglass worm gear set are in line contacts. Computer graphs of the ZN-type hourglass worm and worm wheel are plotted based on the developed mathematical model of worm gear sets. In addition, tooth working surface, contact lines and boundary of the contact lines of the ZN-type hourglass worm wheel are also investigated and compared with those of the ZA-type. It is found that the contact zone of the ZN-type hourglass worm gear set is increased more than twice of that of the ZA-type with an increase of its lead angle to 30°. The increase of pressure angle and normal module of the hourglass worm gear set also results in the increase of its tooth working surface. The proposed analysis procedures and the developed computer aided simulation programs are most helpful to the design and contact analysis of hourglass worm gear sets.

2. Mathematical model of the straight-edged cutting blade

Fig. 1 shows the normal section of the straight-edged cutting blade. It is noted that the ZN-type hourglass worm is generated by a straight-edged cutting blade with upper and lower fillets. The straight-edged cutting blade, which generates the working tooth surfaces, can be expressed in the blade coordinate system $S_c(X_c,Y_c,Z_c)$ by

$$\mathbf{R}_c = \begin{bmatrix} x_c \\ y_c \\ z_c \end{bmatrix} = \begin{bmatrix} \pm(u_1 \sin\alpha - R_0 \cos\alpha) \\ u_1 \cos\alpha + R_0 \sin\alpha \\ 0 \end{bmatrix}, \tag{1}$$

where $u_1 = |\overline{M_0M_1}|$ is a surface parameter of the straight-edged cutting blade and its effective range is $u_{min} \leqslant u_1 \leqslant u_{max}$. Two straight-edged lines are tangent to the cutter's base circle of radius R_0. Design parameter α is the pressure angle of the cutter formed by the straight-edged cutting blade and Y_c-axis. The upper "±" sign of x_c, expressed in Eq. (1), is associated with the left-hand side cutter blade while the lower sign is associated with the right-hand side cutter blade. Similarly, the upper and lower fillets of the normal section of the straight-edged cutting blade, which generate the lower and upper fillet surfaces of the worm, can be expressed in coordinate system $S_c(X_c,Y_c,Z_c)$ as follows:

$$\mathbf{R}_c^{(u)} = \begin{bmatrix} x_c \\ y_c \\ z_c \end{bmatrix} = \begin{bmatrix} \mp(\rho \sin\varphi + (R_0 \cos\alpha - u_1 \sin\alpha - \rho\cos\alpha)) \\ R_0 \sin\alpha + u_1 \cos\alpha - \rho \sin\alpha + \rho\cos\varphi \\ 0 \end{bmatrix}, \tag{2}$$

$$\text{and} \quad \mathbf{R}_c^{(l)} = \begin{bmatrix} x_c \\ y_c \\ z_c \end{bmatrix} = \begin{bmatrix} \pm(\rho \sin\varphi - (R_0 \cos\alpha - u_1 \sin\alpha + \rho\cos\alpha)) \\ R_0 \sin\alpha + u_1 \cos\alpha + \rho \sin\alpha - \rho\cos\varphi \\ 0 \end{bmatrix}, \tag{3}$$

where $0 \leqslant \varphi \leqslant (90^\circ - \alpha)$ and superscripts "u" and "l" denote the upper and lower fillet surfaces of the hourglass worm. Herein, φ is the design parameter that determines the coordinates of any point on this cutter fillet, and ρ represents the design

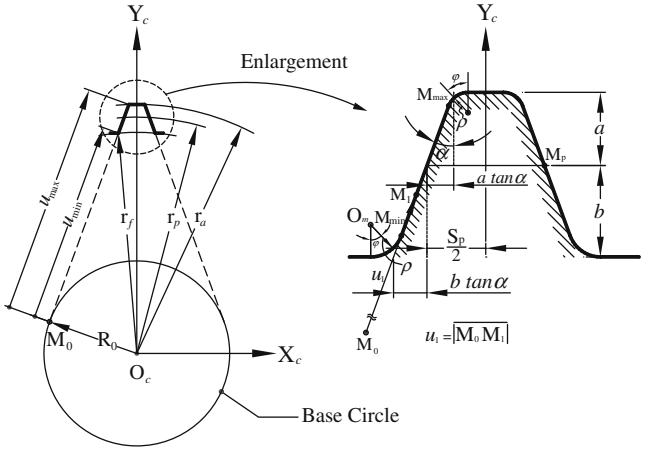

Fig. 1. Geometry of the straight-edged cutting blade.

parameter of fillet radius. The upper "±" signs of Eqs. (2) and (3) indicate the left-side fillet while the lower signs represent the right-side fillet.

Fig. 2 shows the schematic generation mechanism for a ZN-type hourglass worm. In Fig. 2, coordinate system $S_b(X_b, Y_b, Z_b)$ represents the blade coordinate system and coordinate system $S_c(X_c, Y_c, Z_c)$ is attached to the straight-edged cutting blade (as shown in Fig. 1) while $S_a(X_a, Y_a, Z_a)$ is the hourglass worm coordinate system, and axes Z_b and Z_a are rotational axes of the cutting blade and the generated hourglass worm, respectively. In the cutting process of an hourglass worm, the normal section of the straight-edged cutting blade should form a lead angle λ with respect to the worm rotational axis Z_a. Therefore, the blade performs a rotational velocity ω_b about axis Z_b while the worm blank rotates about axis Z_a with a rotational velocity ω_1. According to Fig. 2a, the normal section of the straight-edged blade cutter can be represented in coordinate system S_b by applying the following homogeneous coordinate transformation matrix equation:

$$\mathbf{R}_b = \mathbf{M}_{bc}\mathbf{R}_c, \tag{4}$$

where

$$\mathbf{M}_{bc} = \begin{bmatrix} \cos\lambda & 0 & \sin\lambda & 0 \\ 0 & 1 & 0 & 0 \\ -\sin\lambda & 0 & \cos\lambda & 0 \\ 0 & 0 & 0 & 1 \end{bmatrix},$$

and $\mathbf{R}_b$ and $\mathbf{R}_c$ denote the position vectors of the normal section of blade cutter surfaces represented in coordinate systems $S_b(X_b, Y_b, Z_b)$ and $S_c(X_c, Y_c, Z_c)$, respectively. $\mathbf{M}_{bc}$ is the homogeneous coordinate transformation matrix transforming the

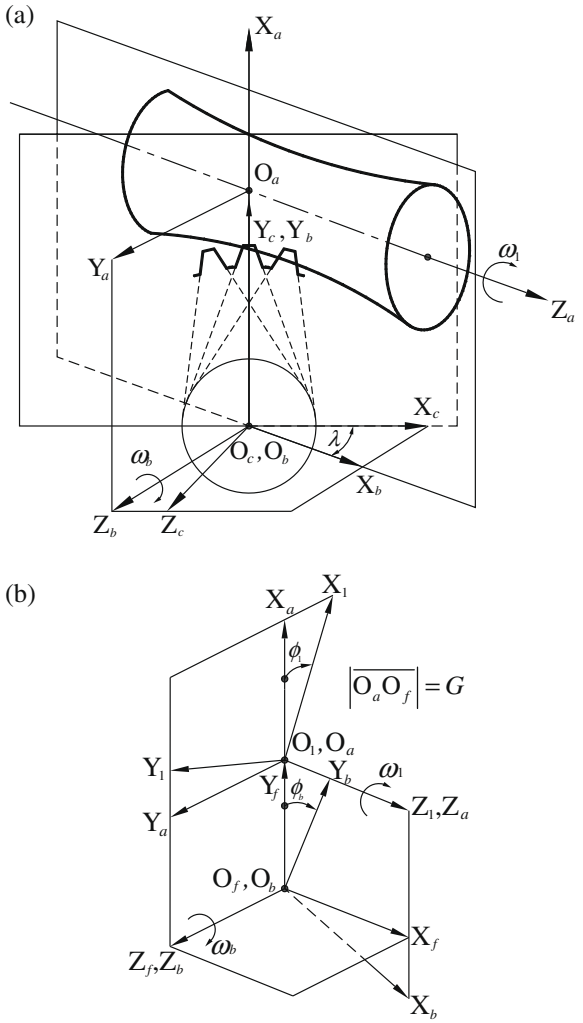

Fig. 2. Coordinate systems between the cutting blade and ZN-type worm.

position vector from coordinate system S_c to S_b. Substituting Eq. (1) into Eq. (4), the profile of straight-edged cutting blade can thus be represented in coordinate system S_b by

$$\mathbf{R}_b = \begin{bmatrix} \pm(u_1 \sin\alpha\cos\lambda - R_0\cos\alpha\cos\lambda) \\ u_1\cos\alpha + R_0\sin\alpha \\ \mp(u_1\sin\alpha\sin\lambda - R_0\cos\alpha\sin\lambda) \end{bmatrix}. \tag{5}$$

Again, the upper sign of "±" sign in Eq. (5) indicates the left-side surface while the lower sign represents the right-side surface. Substituting Eqs. (2) and (3) into Eq. (4) yields the upper and lower fillet surfaces of the blade cutter represented in coordinate system S_b as follows:

$$\mathbf{R}_b^{(u)} = \begin{bmatrix} \mp\cos\lambda(\rho\sin\varphi + R_0\cos\alpha - u_1\sin\alpha - \rho\cos\alpha) \\ R_0\sin\alpha + u_1\cos\alpha - \rho\sin\alpha + \rho\cos\varphi \\ \pm\sin\lambda(\rho\sin\varphi + R_0\cos\alpha - u_1\sin\alpha - \rho\cos\alpha) \end{bmatrix}, \tag{6}$$

$$\text{and} \quad \mathbf{R}_b^{(l)} = \begin{bmatrix} \pm\cos\lambda(\rho\sin\varphi - R_0\cos\alpha + u_1\sin\alpha - \rho\cos\alpha) \\ R_0\sin\alpha + u_1\cos\alpha + \rho\sin\alpha - \rho\cos\varphi \\ \mp\sin\lambda(\rho\sin\varphi - R_0\cos\alpha + u_1\sin\alpha - \rho\cos\alpha) \end{bmatrix}. \tag{7}$$

The upper sign of "±" sign in Eqs. (6) and (7) indicates the left-side fillet surfaces while the lower sign represents the right-side fillet surfaces.

3. Mathematical model of the ZN-type hourglass worm

Fig. 2b shows the schematic generation mechanism for an hourglass worm, where coordinate system $S_b(X_b, Y_b, Z_b)$ denotes the cutting blade coordinate system, $S_1(X_1, Y_1, Z_1)$ is attached to the worm, $S_f(X_f, Y_f, Z_f)$ is the fixed coordinate system, and $S_a(X_a, Y_a, Z_a)$ is the reference coordinate system. In the generation process of an hourglass worm, coordinate system $S_b(X_b, Y_b, Z_b)$ of the cutting blade rotates about Z_b-axis through an angle ϕ_b while coordinate system $S_1(X_1, Y_1, Z_1)$ of the worm rotates about Z_1-axis through an angle ϕ_1. The locus of the cutting blade can be represented in the worm coordinate system $S_1(X_1, Y_1, Z_1)$ by applying the following homogeneous coordinate transformation matrix equation:

$$\mathbf{R}_1 = \mathbf{M}_{1a}\mathbf{M}_{af}\mathbf{M}_{fb}\mathbf{R}_b = \mathbf{M}_{1b}\mathbf{R}_b, \tag{8}$$

where

$$\mathbf{M}_{1b} = \begin{bmatrix} -\cos\phi_1\sin\phi_b & \cos\phi_1\cos\phi_b & -\sin\phi_1 & -G\cos\phi_1 \\ -\sin\phi_1\sin\phi_b & \sin\phi_1\cos\phi_b & \cos\phi_1 & -G\sin\phi_1 \\ \cos\phi_b & \sin\phi_b & 0 & 0 \\ 0 & 0 & 0 & 1 \end{bmatrix}. \tag{9}$$

The rotation axes between the hourglass worm and cutting blade are crossed axes, and the shortest distance between these two axes is G. That is

$$G = r_b + r_1, \tag{10}$$

where r_b and r_1 are the pitch radii of cutter blade and hourglass worm, respectively. The ratio m_{1b} of the angular velocities of hourglass worm and cutter blade is defined as:

$$m_{1b} = \frac{\omega_1}{\omega_b} = \frac{\phi_1}{\phi_b} = \frac{T_b}{T_1}, \tag{11}$$

where $\omega_1 = \frac{d\phi_1}{dt}$, $\omega_b = \frac{d\phi_b}{dt}$, and T_1 and T_b are the numbers of worm threads and cutter teeth, respectively.

Substituting Eqs. (5) and (9) into Eq. (8), the surface equation of the ZN-type hourglass worm $\mathbf{R}_1$, represented in coordinate system $S_1(X_1, Y_1, Z_1)$, can be expressed as follows:

$$\mathbf{R}_1(u_1, \phi_1) = \begin{bmatrix} (\mp\cos\phi_1\sin\phi_b)x_b + (\cos\phi_1\cos\phi_b)y_b \mp \sin\phi_1 z_b - G\cos\phi_1 \\ (\mp\sin\phi_1\sin\phi_b)x_b + (\sin\phi_1\cos\phi_b)y_b \pm \cos\phi_1 z_b - G\sin\phi_1 \\ \cos\phi_b x_b + \sin\phi_b y_b \end{bmatrix}, \tag{12}$$

where u_1 and ϕ_1 are surface parameters of the hourglass worm. In Eq. (12), the upper sign of "±" sign represents the left-side hourglass worm surface while the lower sign indicates the right-side hourglass worm surface. Similarly, substituting Eqs. (6), (7), and (9) into Eq. (8), the vector equations of upper and lower fillet surfaces of the ZN-type hourglass worm $\mathbf{R}_1^{(u)}$ and $\mathbf{R}_1^{(l)}$, represented in coordinate system $S_1(X_1, Y_1, Z_1)$, can be expressed by

$$\mathbf{R}_1^{(u)}(\varphi, \phi_1) = \begin{bmatrix} (\pm\cos\phi_1\sin\phi_b)x_b^{(u)} + (\cos\phi_1\cos\phi_b)y_b^{(u)} \mp \sin\phi_1 z_b^{(u)} - G\cos\phi_1 \\ (\pm\sin\phi_1\sin\phi_b)x_b^{(u)} + (\sin\phi_1\cos\phi_b)y_b^{(u)} \pm \cos\phi_1 z_b^{(u)} - G\sin\phi_1 \\ \mp\cos\phi_b x_b^{(u)} + \sin\phi_b y_b^{(u)} \end{bmatrix}, \tag{13}$$

$$\text{and}\quad \mathbf{R}_1^{(l)}(\varphi,\phi_1)=\begin{bmatrix}(\mp\cos\phi_1\sin\phi_b)x_b^{(l)}+(\cos\phi_1\cos\phi_b)y_b^{(l)}\pm\sin\phi_1 z_b^{(l)}-G\cos\phi_1\\(\mp\sin\phi_1\sin\phi_b)x_b^{(l)}+(\sin\phi_1\cos\phi_b)y_b^{(l)}\mp\cos\phi_1 z_b^{(l)}-G\sin\phi_1\\\pm\cos\phi_b x_b^{(l)}+\sin\phi_b y_b^{(l)}\end{bmatrix}, \tag{14}$$

where φ and ϕ_1 are surface parameters of the hourglass worm fillets. In Eqs. (13) and (14), the upper "±" sign represents the left-side fillet surfaces while the lower sign indicates the right-side fillet surfaces.

The surface normal vector $\mathbf{N}_1$, $\mathbf{N}_1^{(u)}$ and $\mathbf{N}_1^{(l)}$ of the hourglass worm can be obtained and represented in coordinate system $S_1(X_1,Y_1,Z_1)$ as follows:

$$\mathbf{N}_1=\frac{\partial\mathbf{R}_1}{\partial u_1}\times\frac{\partial\mathbf{R}_1}{\partial\phi_1}(\text{for working surfaces generated by the straight-edge blade cutter}), \tag{15}$$

$$\mathbf{N}_1^{(u)}=\frac{\partial\mathbf{R}_1^{(u)}}{\partial\varphi}\times\frac{\partial\mathbf{R}_1^{(u)}}{\partial\phi_1}(\text{for upper fillet surfaces}), \tag{16}$$

$$\text{and}\quad \mathbf{N}_1^{(l)}=\frac{\partial\mathbf{R}_1^{(l)}}{\partial\varphi}\times\frac{\partial\mathbf{R}_1^{(l)}}{\partial\phi_1}(\text{for lower fillet surfaces}), \tag{17}$$

where

$$\frac{\partial\mathbf{R}_1}{\partial u_1}=\begin{bmatrix}(\mp\sin\alpha\cos\lambda\sin\phi_b+\cos\alpha\cos\phi_b)\cos\phi_1\pm\sin\alpha\sin\lambda\sin\phi_1\\(\mp\sin\alpha\cos\lambda\sin\phi_b+\cos\alpha\cos\phi_b)\sin\phi_1\mp\sin\alpha\sin\lambda\cos\phi_1\\\pm(\sin\alpha\cos\lambda\sin\phi_b+\cos\alpha\sin\phi_b)\end{bmatrix},$$

$$\frac{\partial\mathbf{R}_1^{(u)}}{\partial\varphi}=\begin{bmatrix}\rho(\cos\phi_1(\pm\sin\varphi\cos\lambda\sin\phi_b-\sin\varphi\cos\phi_b))\mp\cos\varphi\sin\lambda\sin\phi_1\\\rho(\sin\phi_1(\pm\cos\varphi\cos\lambda\sin\phi_b-\sin\varphi\cos\phi_b))\pm\cos\varphi\sin\lambda\cos\phi_1\\\rho(\mp\cos\varphi\cos\lambda\cos\phi_b-\sin\varphi\sin\phi_b)\end{bmatrix},$$

$$\frac{\partial\mathbf{R}_1^{(l)}}{\partial\varphi}=\begin{bmatrix}\rho(\cos\phi_1(\mp\sin\varphi\cos\lambda\sin\phi_b+\sin\varphi\cos\phi_b))\pm\cos\varphi\sin\lambda\sin\phi_1\\\rho(\sin\phi_1(\mp\cos\varphi\cos\lambda\sin\phi_b+\sin\varphi\cos\phi_b))\mp\cos\varphi\sin\lambda\cos\phi_1\\\rho(\pm\cos\varphi\cos\lambda\cos\phi_b+\sin\varphi\sin\phi_b)\end{bmatrix},$$

$$\frac{\partial\mathbf{R}_1}{\partial\phi_1}=\frac{\partial\mathbf{R}_1^{(u)}}{\partial\phi_1}=\frac{\partial\mathbf{R}_1^{(l)}}{\partial\phi_1}=\begin{bmatrix}\pm A_1^{(k)}(\cos\lambda\sin\phi_1\sin\phi_b-m_{b1}\cos\lambda\cos\phi_1\cos\phi_b+\sin\lambda\cos\phi_1)\\-A_2^{(k)}(\sin\phi_1\cos\phi_b-m_{b1}\cos\phi_1\sin\phi_b)+G\sin\phi_1\\\mp A_1^{(k)}(\cos\lambda\cos\phi_1\sin\phi_b+m_{b1}\cos\lambda\sin\phi_1\cos\phi_b-\sin\lambda\sin\phi_1)\\+A_2^{(k)}(\cos\phi_1\cos\phi_b-m_{b1}\sin\phi_1\sin\phi_b)-G\cos\phi_1\\m_{b1}(\mp A_1^{(k)}\cos\lambda\sin\phi_b+A_2^{(k)}\cos\phi_b)\end{bmatrix},$$

$(k=b,u\text{ and }l)$,

$A_1^{(b)}=u_1\sin\alpha-R_0\cos\alpha$,

$A_2^{(b)}=u_1\cos\alpha+R_0\sin\alpha$,

$A_1^{(u)}=-\rho\sin\varphi-(R_0\cos\alpha-u_1\sin\alpha-\rho\cos\alpha)$,

$A_2^{(u)}=R_0\sin\alpha+u_1\cos\alpha-\rho\sin\alpha+\rho\cos\varphi$,

$A_1^{(l)}=\rho\sin\varphi-(R_0\cos\alpha-u_1\sin\alpha+\rho\cos\alpha)$,

and $A_2^{(l)}=R_0\sin\alpha+u_1\cos\alpha+\rho\sin\alpha-\rho\cos\varphi$.

Herein superscripts "*b*", "*u*" and "*l*" denote the working surface, upper fillet surface and lower fillet surface of the hourglass worm, respectively.

According to Eqs. (15)–(17), surface normals of the ZN-type hourglass worm surfaces and fillet surfaces can be attained as follows:

$$\begin{aligned}N_{1x}&=(D_1^{(k)}\sin\phi_1\mp D_2^{(k)}\cos\phi_1)[(\mp A_1^{(k)}\cos\lambda\sin\phi_b+A_2^{(k)}\cos\phi_b)m_{b1}]-(\pm E_1^{(k)})(\mp A_1^{(k)}C_1+A_2^{(k)}C_2-G\cos\phi_1),\\N_{1y}&=(E_1^{(k)})(\pm A_1^{(k)}B_1-A_2^{(k)}B_2+G\sin\phi_1)-(D_1^{(k)}\cos\phi_1\pm D_2^{(k)}\sin\phi_1)[(\mp A_1^{(k)}\cos\lambda\sin\phi_b+A_2^{(k)}\cos\phi_b)m_{b1}],\\\text{and }N_{1z}&=(D_1^{(k)}\cos\phi_1\pm D_2^{(k)}\sin\phi_1)(\mp A_1^{(k)}C_1+A_2^{(k)}C_2-G\cos\phi_1)-(D_1^{(k)}\sin\phi_1\mp D_2^{(k)}\cos\phi_1)(\pm A_1^{(k)}B_1-A_2^{(k)}B_2+G\sin\phi_1),\end{aligned} \tag{18}$$

where superscript $k=b$, u and l,

$B_1^{(b)}=B_1^{(u)}=B_1^{(l)}=\cos\lambda\sin\phi_1\sin\phi_b-m_{b1}\cos\lambda\cos\phi_1\cos\phi_b+\sin\lambda\cos\phi_1$,

$B_2^{(b)}=B_2^{(u)}=B_2^{(l)}=\sin\phi_1\cos\phi_b-m_{b1}\cos\phi_1\sin\phi_b$,

$$C_1^{(b)} = C_1^{(u)} = C_1^{(l)} = \cos\lambda\cos\phi_1\sin\phi_b + m_{b1}\cos\lambda\sin\phi_1\cos\phi_b - \sin\lambda\sin\phi_1,$$
$$C_2^{(b)} = C_2^{(u)} = C_2^{(l)} = \cos\phi_1\cos\phi_b - m_{b1}\sin\phi_1\sin\phi_b,$$
$$D_1^{(b)} = \mp\sin\alpha\cos\lambda\sin\phi_b + \cos\alpha\cos\phi_b,$$
$$D_2^{(b)} = \sin\alpha_n\sin\lambda,$$
$$D_1^{(u)} = \rho(\pm\cos\varphi\cos\lambda\sin\phi_b - \sin\varphi\cos\phi_b),$$
$$D_2^{(u)} = \cos\varphi\sin\lambda,$$
$$D_1^{(l)} = \rho(\mp\cos\varphi\cos\lambda\sin\phi_b + \sin\varphi\cos\phi_b),$$
$$D_2^{(l)} = \cos\varphi\sin\lambda,$$
$$E_1^{(b)} = \sin\alpha\cos\lambda\sin\phi_b + \cos\alpha\sin\phi_b,$$
$$E_1^{(u)} = \mp\cos\varphi\cos\lambda\cos\phi_b - \sin\varphi\sin\phi_b,$$
$$\text{and}\quad E_1^{(l)} = \pm\cos\varphi\cos\lambda\cos\phi_b + \sin\varphi\sin\phi_b.$$

In Eq. (18), the upper sign of "±" sign represents the left-side worm surface while the lower sign indicates the right-side worm surface.

4. Computer graph of the ZN-type hourglass worm

Table 1 lists some major design parameters of the ZN-type hourglass worm and blade cutter. It is noted that λ is the lead angle of the worm in the middle plane (the section of the minimal diameter) of the worm, and it is changing along the worm axis. Based on the developed mathematical model of the ZN-type hourglass worm, a three-dimensional tooth profile of the ZN-type hourglass worm is plotted as shown in Fig. 3. Coordinates of the hourglass worm surface points can also be calculated by applying the developed mathematical model.

5. Equation of meshing of the hourglass worm-type hob cutter and worm wheel

An hourglass worm-type hob cutter, which is identical to the ZN-type hourglass worm, is used for the generation of hourglass worm wheel. The schematic cutting mechanism of an hourglass worm wheel is shown in Fig. 4. Coordinate system

Table 1
Major design parameters of the ZN-type hourglass worm and blade cutter.

Items	Parameters	
Lead angle of the blade cutter (Fig. 2a)	λ	5.0°
Normal pressure angle of the blade cutter	α	20.0°
Normal module of the blade cutter	m_n	2.0 mm/tooth
Pitch circle radius of the blade cutter	r_p	47.04 mm
Base circle radius of the blade cutter	r_b	21.92 mm
Number of thread of the worm	T_1	1
Lead angle of the worm	λ	5.0°
Pitch circle radius of the worm	r_1	22.0 mm
Cross angle of the worm gear set	γ	90.0°

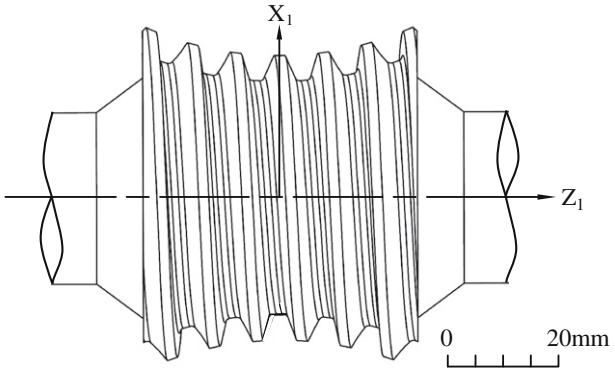

Fig. 3. Computer graph of the ZN-type hourglass worm.

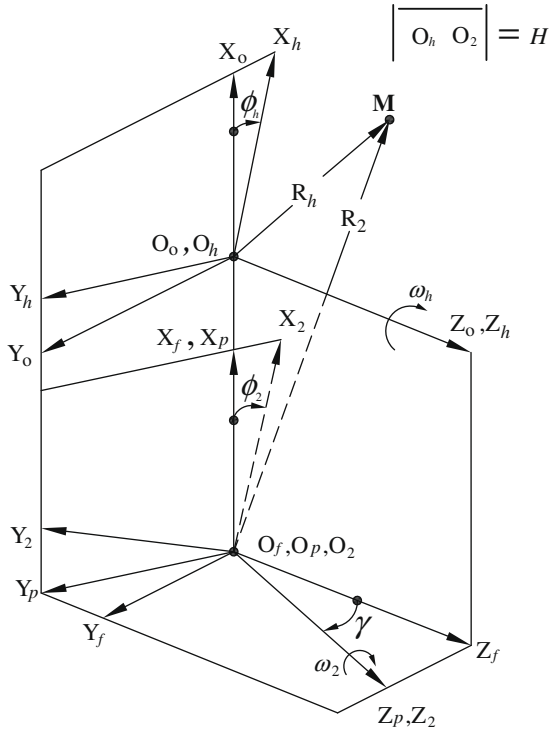

Fig. 4. Schematic cutting mechanism of an hourglass worm wheel.

$S_h(X_h,Y_h,Z_h)$ is associated with the hourglass worm-type hob cutter, $S_2(X_2,Y_2,Z_2)$ is attached to the hourglass worm wheel, $S_o(X_o,Y_o,Z_o)$ and $S_p(X_p,Y_p,Z_p)$ are the reference coordinate systems for the hourglass worm-type hob cutter and worm wheel, respectively, and $S_f(X_f,Y_f,Z_f)$ is the fixed coordinate system. Axes Z_h and Z_2 are rotation axes of the ZN-type hourglass worm-type hob cutter and worm wheel, respectively. Parameter γ measured from Z_f-axis to Z_p-axis, is the cross angle of the hourglass hob cutter and worm wheel. Parameter H is the shortest center distance of these two rotation axes, and it can be expressed by

$$H = r_h + r_2, \tag{19}$$

where r_h and r_2 are the pitch radii of the hourglass worm-type hob cutter and worm wheel, respectively.

In Fig. 4, ϕ_h and ϕ_2 are the rotation angles of the hourglass worm-type hob cutter and worm wheel, respectively, during the cutting process. Therefore, angular velocity of the worm wheel can be expressed in reference coordinate system $S_p(X_p,Y_p,Z_p)$ by

$$\boldsymbol{\omega}_2^{(p)} = \frac{d\phi_2}{dt}\mathbf{k}^{(p)} = \omega_2\mathbf{k}^{(p)}, \tag{20}$$

where symbol $\mathbf{k}^{(p)}$ denotes the unit vector of Z_p-axis. This angular velocity can also be represented in coordinate system $S_h(X_h,Y_h,Z_h)$ as follows:

$$\boldsymbol{\omega}_2^{(h)} = \mathbf{L}_{hp}\boldsymbol{\omega}_2^{(p)} = \begin{bmatrix} \cos\phi_h & -\sin\phi_h\cos\gamma & -\sin\phi_h\sin\gamma \\ \sin\phi_h & \cos\phi_h\cos\gamma & \cos\phi_h\sin\gamma \\ 0 & -\sin\gamma & \cos\gamma \end{bmatrix}\begin{bmatrix} 0 \\ 0 \\ -\omega_2 \end{bmatrix} = \omega_h\begin{bmatrix} -m_{2h}\sin\phi_h\sin\gamma \\ m_{2h}\cos\phi_h\sin\gamma \\ m_{2h}\cos\gamma \end{bmatrix}, \tag{21}$$

where $m_{2h} = \frac{\omega_2}{\omega_h}$.

The angular velocity of the hourglass worm-type hob cutter represented in coordinate system $S_h(X_h,Y_h,Z_h)$ is

$$\boldsymbol{\omega}_h^{(h)} = -\frac{d\phi_h}{dt}\mathbf{k}^{(h)} = -\omega_h\mathbf{k}^{(h)}. \tag{22}$$

The position vector of the shortest axial distance $|\mathbf{O}_h\mathbf{O}_2|$ can also be represented in coordinate system $S_h(X_h,Y_h,Z_h)$ by

$$\mathbf{O}_h\mathbf{O}_2^{(h)} = \begin{bmatrix} -H\cos\phi_h \\ -H\sin\phi_h \\ 0 \end{bmatrix}. \tag{23}$$

According to Eqs. (21)–(23), the relative velocity of hourglass worm-type hob cutter and worm wheel, represented in coordinate system S_h, can be obtained by applying the following equation:

$$\mathbf{V}_{h2}^{(h)} = (\boldsymbol{\omega}_h^{(h)} - \boldsymbol{\omega}_2^{(h)}) \times \mathbf{R}_h - \mathbf{O}_h\mathbf{O}_2^{(h)} \times \boldsymbol{\omega}_2^{(h)}, \tag{24}$$

where $\mathbf{R}_h$ is the position vector of common contact point of the hob cutter and worm wheel, represented in coordinate system S_h, as expressed in Eq. (12). Substituting Eqs. (12), (21), (22), and (23) into Eq. (24), the relative velocity of the hourglass worm-type hob cutter and worm wheel can be obtained as follows:

$$\mathbf{V}_{h2}^{(h)} = \begin{bmatrix} -R_{hz}m_{2h}\sin\gamma\cos\phi_h - R_{hy}(-1-m_{2h}\cos\gamma) + Hm_{2h}\sin\phi_h\cos\gamma \\ R_{hx}(-1-m_{2h}\cos\gamma) - R_{hz}m_{2h}\sin\gamma\sin\phi_h - Hm_{2h}\cos\phi_h\cos\gamma \\ R_{hy}m_{2h}\sin\gamma\sin\phi_h + R_{hx}m_{2h}\sin\gamma\cos\phi_h + Hm_{2h}\cos^2\phi_h\sin\gamma + Hm_{2h}\sin^2\phi_h\sin\gamma \end{bmatrix}. \tag{25}$$

Due to conjugate action between the hob cutter and worm wheel, the relative velocity $\mathbf{V}_{h2}^{(h)}$ is perpendicular to the common surface normal $\mathbf{N}_h$, where $\mathbf{N}_h = \mathbf{N}_1$. Hence, the following equation must be observed:

$$\mathbf{N}_h \cdot \mathbf{V}_{h2}^{(h)} = 0. \tag{26}$$

Substituting Eqs. (18) and (25) into Eq. (26) yields:

$$\begin{aligned} f(u_1,\phi_1,\phi_h) = {} & \left\{(D_1^{(k)}\sin\phi_1 \mp D_2^{(k)}\cos\phi_1)[(\mp A_1^{(k)}\cos\lambda\sin\phi_b + A_2^{(k)}\cos\phi_b)m_{b1}]\right. \\ & \left.-(\pm E_1^{(k)})(\mp A_1^{(k)}C_1 + A_2^{(k)}C_2 - G\cos\phi_1)\right\}\left[-R_{hz}m_{2h}\sin\gamma\cos\phi_h - R_{hy}(-1-m_{2h}\cos\gamma) + Hm_{2h}\sin\phi_h\cos\gamma\right] \\ & + \left\{(\pm E_1^{(k)})(\pm A_1^{(k)}B_1 - A_2^{(k)}B_2 + G\sin\phi_1) - (D_1^{(k)}\cos\phi_1 \pm D_2^{(k)}\sin\phi_1)\right. \\ & \left.+\left[(\mp A_1^{(k)}\cos\lambda\sin\phi_b + A_2^{(k)}\cos\phi_b)m_{b1}\right]\right\}\left[R_{hx}(-1-m_{2h}\cos\gamma) - R_{hz}m_{2h}\sin\gamma\sin\phi_h - Hm_{2h}\cos\phi_h\cos\gamma\right] \\ & + \left\{(D_1^{(k)}\cos\phi_1 \pm D_2^{(k)}\sin\phi_1)(\mp A_1^{(k)}C_1 + A_2^{(k)}C_2 - G\cos\phi_1)\right. \\ & \left.-(D_1^{(k)}\sin\phi_1 \mp D_2^{(k)}\cos\phi_1)(\pm A_1^{(k)}B_1 - A_2^{(k)}B_2 + G\sin\phi_1)\right\} \\ & \times\left(R_{hy}m_{2h}\sin\gamma\sin\phi_h + R_{hx}m_{2h}\sin\gamma\cos\phi_h + Hm_{2h}\cos^2\phi_h\sin\gamma + Hm_{2h}\sin^2\phi_h\sin\gamma\right) = 0. \end{aligned} \tag{27}$$

Equation (27) is the so-call equation of meshing that relates the surface parameters of hourglass worm-type hob cutter to the cutting motion parameters of the generated hourglass worm wheel.

6. Mathematical model of the ZN-type hourglass worm wheel surface

According to the coordinate systems shown in Fig. 4, the locus of the hourglass worm-type hob cutter can be represented in coordinate system S_2 by

$$\mathbf{R}_2(u_1,\phi_1,\phi_h) = \mathbf{M}_{2p}\mathbf{M}_{pf}\mathbf{M}_{fo}\mathbf{M}_{oh}\mathbf{R}_h(u_1,\phi_1) = \mathbf{M}_{2h}\mathbf{R}_h(u_1,\phi_1), \tag{28}$$

where

$$\mathbf{M}_{2h} = \begin{bmatrix} a11 & a12 & \sin\phi_2\sin\gamma & H\cos\phi_2 \\ b21 & b22 & -\cos\phi_2\sin\gamma & H\sin\phi_2 \\ -\sin\gamma\sin\phi_h & \sin\gamma\cos\phi_h & \cos\gamma & 0 \\ 0 & 0 & 0 & 1 \end{bmatrix}, \tag{29}$$

$a11 = \cos\phi_2\cos\phi_h + \sin\phi_2\cos\gamma\sin\phi_h,$
$a12 = \cos\phi_2\sin\phi_h - \sin\phi_2\cos\gamma\cos\phi_h,$
$b21 = \sin\phi_2\cos\phi_h - \cos\phi_2\cos\gamma\sin\phi_h,$
and $\quad b22 = \sin\phi_2\sin\phi_h + \cos\phi_2\cos\gamma\cos\phi_h.$

Parameter γ represents the cross angle of the ZN-type hourglass worm gear set. Since the geometry of the hourglass worm-type hob cutter is identical to that of the ZN-type hourglass worm, the position vector $\mathbf{R}_1 = \mathbf{R}_h$ and normal vector $\mathbf{N}_1 = \mathbf{N}_h$. Substituting Eqs. (12), (13), (14), and (29) into Eq. (28), the locus equations of the hourglass worm-type hob cutter can be represented in worm wheel coordinate system S_2 as follows:

$$\begin{aligned} x_2 &= (\cos\phi_2\cos\phi_h + \sin\phi_2\cos\gamma\sin\phi_h)R_{hx} + (\cos\phi_2\sin\phi_h - \sin\phi_2\cos\gamma\cos\phi_h)R_{hy} + \sin\phi_2\sin\gamma R_{hz} + H\cos\phi_2, \\ y_2 &= (\sin\phi_2\cos\phi_h - \cos\phi_2\cos\gamma\sin\phi_h)R_{hx} + (\sin\phi_2\sin\phi_h + \cos\phi_2\cos\gamma\cos\phi_h)R_{hy} - \cos\phi_2\sin\gamma R_{hz} + H\sin\phi_2, \\ \text{and}\quad z_2 &= -\sin\gamma\sin\phi_h R_{hx} + \sin\gamma\cos\phi_h R_{hy} + \cos\gamma R_{hz}. \end{aligned} \tag{30}$$

where parameters R_{hx}, R_{hy} and R_{hz} are defined similar to those represented in Eqs. (12)–(14) due to $\mathbf{R}_1 = \mathbf{R}_h$. The mathematical model of the ZN-type hourglass worm wheel surface can be obtained by considering Eqs. (27) and (30), simultaneously.

7. Computer graph of the ZN-type hourglass worm wheel

It is recalled that Eq. (12) defines the left-side and right-side tooth surfaces of the ZN-type hourglass worm while Eqs. (27) and (30) represent the left-side and right-side tooth surfaces of the ZN-type hourglass worm wheel. Table 2 shows some major design parameters for the ZN-type hourglass worm gear set. The coordinates of worm wheel tooth surface points can be calculated by applying the developed mathematical model of the worm wheel. A three-dimensional hourglass worm wheel is plotted, as shown in Fig. 5.

8. Tooth working surface of the ZN-type hourglass worm wheel

Design parameters of the ZN-type hourglass worm wheel are chosen the same as those listed in Table 2. Fig. 6 shows the contact lines and boundary lines of the hourglass worm gear set, which define the tooth working regions, on the tooth surfaces of the ZN-type and ZA-type hourglass worm wheels. It is noted that the hourglass worm wheel surface is divided into three regions. Tooth surface regions I and III of the hourglass worm wheel are generated by the first working cutting edge of the hourglass worm-type hob cutter. Region II of the worm wheel tooth surface is the envelope to the family of contact lines of the hourglass worm gear set. Region II also indicates the tooth working area or contact region of the worm and worm wheel surfaces. When the rotation angle ϕ_b of the cutting blade equals 0.0°, regions II and III of the ZN-type worm wheel tooth surface are separated by the straight line $\overline{CC'}$ while the ZA-type worm wheel tooth surface is separated by the line $\overline{AA'}$ which lies on the section $Z_2 = 0$ mm (refer to Figs. 5 and 6) of the tooth surface. When the rotation angle ϕ_b of the cutting blade equals $-\alpha$(i.e. -20.0°), regions I and II of the ZN-type worm wheel tooth surface are separated by the curve line $\widehat{DD'}$ while the ZA-type worm wheel tooth surface is separated by the curve line $\widehat{BB'}$ which is generated by the edge of the hob cutter. Where $\overline{AA'}$ and $\widehat{BB'}$ lines are called the boundary lines of contact or the envelope of contact lines for the ZA-type hourglass worm wheel surface. Similarly, $\overline{CC'}$ and $\widehat{DD'}$ are the boundary lines of contact of the ZN-type hourglass worm wheel surface. Based on the contact lines shown in enlargement figure (Fig. 6), there has a slightly sharp edge between regions II and III, and it is unfavorable for the elastohydrodynamic lubrication of the hourglass worm gear drive.

Table 2
Major parameters of the ZN-type hourglass worm-type hob cutter and worm wheel.

Item	Parameters	
Number of teeth of hourglass worm-type hob cutter	T_h	1
Lead angle of hourglass worm-type hob cutter	λ	5.0°
Normal pressure angle of hourglass worm-type hob cutter	α	20.0°
Normal module of hourglass worm-type hob cutter	m_n	2.0 mm/tooth
Pitch radius of hourglass worm-type hob cutter	r_h	22.0 mm
Number of teeth of worm wheel	T_2	47
Pitch radius of worm wheel	r_2	47.04 mm
Outside radius of worm wheel	r_{2a}	48.64 mm
Cross angle of the worm gear set	γ	90.0°

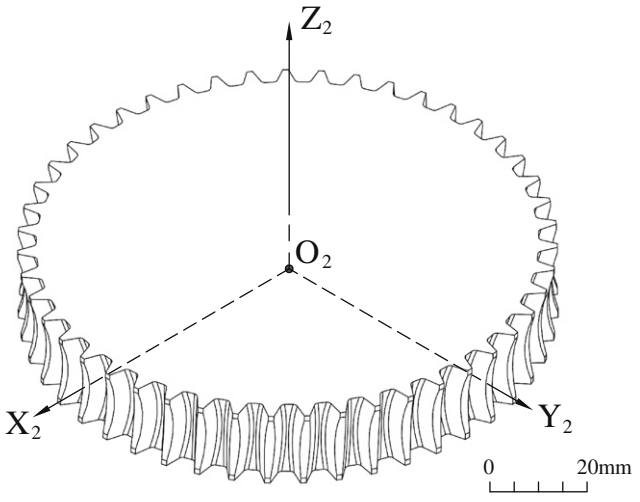

Fig. 5. Computer graph of the ZN-type hourglass worm wheel.

Fig. 7 shows three regions of the hourglass worm wheel tooth surface that are generated by a worm-type hourglass hob cutter with different lead angles $\lambda = 0^\circ, \lambda = 5.0^\circ$ and $\lambda = 30.0^\circ$, respectively. It is found that the area of region II (i.e. tooth working surface) reaches its minimum when the worm wheel surface is generated by a ZA-type hourglass hob cutter (i.e. lead angle $\lambda = 0^\circ$). If the tooth width of the hourglass worm wheel is chosen as $W = 16$ mm, the area of region II is 7.82% of the ZA-type worm wheel tooth surface. Nevertheless, when the lead angles of the ZN-type hourglass worm-type hob cutters are chosen as $\lambda = 5.0^\circ$ and 30.0°, the areas of region II are 9.62% and 16.93% of the ZN-type worm wheel tooth surface, respectively. Thus, the envelope of contact lines (i.e. region II) on the hourglass worm wheel tooth surface will be increased with the increase of lead angles of the hourglass worm-type hob cutter.

If the normal module, m_n, of the worm wheel is changed from 2.0 mm/tooth to 4.0 mm/tooth and the tooth width $W = 16$ mm remains the same, the surface boundary lines of regions I, II and III are shown in Fig. 8. Since the module is increased from 2.0 mm/tooth to 4.0 mm/tooth, the whole face height and area of region II will also be increased. The envelope

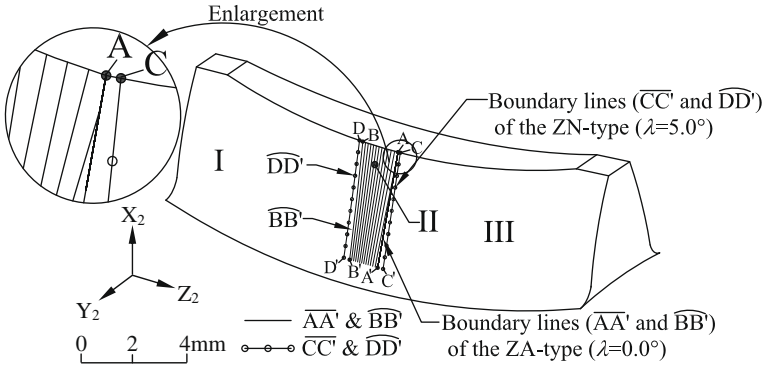

Fig. 6. Contact lines and boundary lines of the hourglass worm wheel surface.

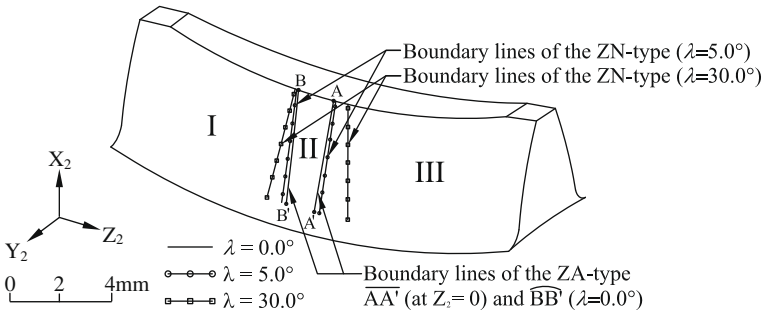

Fig. 7. Boundary lines of worm wheel tooth working surface (m_n = 2.0 mm/tooth) under different lead angles.

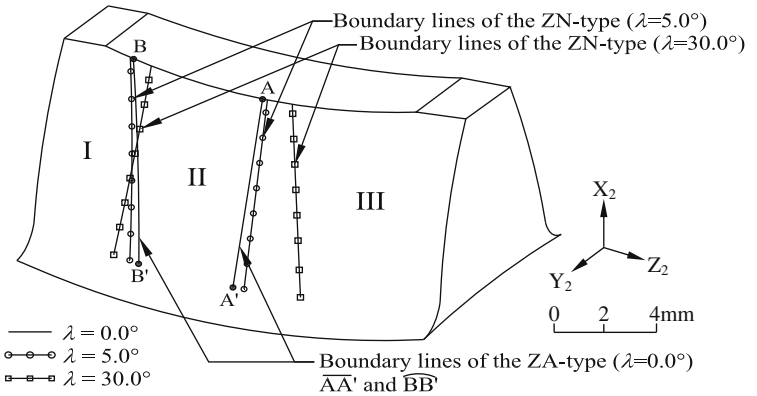

Fig. 8. Boundary lines of the worm wheel tooth working surface with m_n = 4.0 mm/tooth and different lead angles.

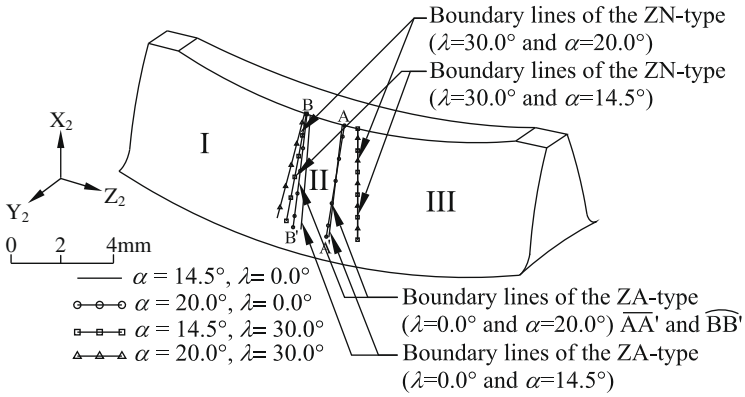

Fig. 9. Boundary lines of worm wheel tooth working surface under different pressure angles.

to contact lines (i.e. area of region II) for m_n = 4.0 mm/tooth is larger than that of m_n = 2.0 mm/tooth under different lead angles, λ, on the worm wheel tooth surface. In this case, the areas of region II are 27.23%, 30.58% and 39.32% of the whole tooth surface under different lead angles $\lambda = 0°, \lambda = 5.0°$ and $\lambda = 30.0°$, respectively.

Boundary lines on the tooth surface of the hourglass worm wheel with different pressure angles α = 14.5° and α = 20.0° under the lead angle $\lambda = 0.0°$ and 30.0°, respectively, are also shown in Fig. 9. It is found that the area of region II of the ZA-type hourglass worm wheel surface is smaller than that of the ZN-type. If the tooth width of the hourglass worm wheel is also chosen as W = 16 mm, the areas of region II are 6.98% and 15.15% of the worm wheel tooth surface, respectively, for the ZA-type and ZN-type hourglass worm wheel tooth surfaces with the pressure angle α = 14.5°. However, the contact zone of the hourglass worm wheel tooth surface will be increased with the increase of pressure angles. The areas of region II are 7.82% and 16.93% of the worm wheel tooth surface, respectively, for the ZA-type and ZN-type hourglass worm wheel tooth surface with the pressure angle α = 20.0°. Therefore, one can increase the lead angle λ, to increase the area of region II of an hourglass worm wheel working surface.

9. Conclusions

The mathematical model of the ZN-type hourglass worm gear set is developed according to the theory of gearing and gear generation mechanism. Computer graphs of the worm and worm wheel are displayed. Tooth surfaces of the ZN-type hourglass worm gear set are expressed in terms of design parameters of the worm-type hourglass hob cutter. The tooth surface of the proposed hourglass worm wheel is the envelope to the two-parameter family of worm-type hourglass hob cutter surfaces.

In this study, the tooth working surface variations of the hourglass worm wheel tooth surfaces with different lead angles, pressure angles and modules are investigated. The area of region II (tooth working surface) of the ZN-type hourglass worm wheel tooth surface, generated by a worm-type hourglass hob cutter with lead angle $\lambda = 30.0°$, is larger than that of the ZA-type hourglass worm wheel (i.e. $\lambda = 0.0°$). In addition, an increase of worm wheel pressure angle α or module m_n will also increase the area of region II of the worm wheel tooth surface. The developed gear tooth mathematical model may help us to explore the possibility for further investigations, such as sensitivity analysis, kinematic errors and contact stress analysis. The analysis results are most helpful to the designers and manufacturers to design and choose proper parameters for hourglass worm gear sets.

Acknowledgments

The authors are grateful to the National Science Council of the ROC for the grant. Part of this work was performed under Contract No. NSC 95-2221-E-159-002-MY3.

References

[1] M. Maki, T. Sakai, A study on hourglass worm gearing with developable tooth surfaces, Journal of Mechanical Design 100 (1978) 451–459.
[2] K. Ishida, Theoretical and experimental investigation of a new plane toothed wheel and its enveloping hourglass worm, Journal of Mechanical Design 100 (1978) 460–469.
[3] M. Maki, T. Sakai, A study on hourglass worm gearing with contact slide-roll ratio, Journal of Mechanical Design 101 (1979) 274–280.
[4] H. Winter, H. Wilkesmann, Calculation of cylindrical worm gear drives of different tooth profiles, Journal of Mechanical Design 103 (1981) 73–82.
[5] V. Simon, Grinding wheel profile for hob relief grinding, Journal of Mechanical Design 104 (1982) 731–742.
[6] V. Simon, Computer aided manufacture of high precision hob, International Journal of machine Tools and Manufacture 28 (4) (1988) 443–452.
[7] V. Simon, Double enveloping worm gear drive with smooth gear tooth surface, in: Proceedings, International Conference on Gearing, Zhengzhou, 1988, pp. 191–194.

[8] V. Simon, A new type of ground double enveloping worm gear drive, in: Proceedings, 1989 ASME Fifth International Power Transmissions and Gearing Conference, Chicago, 1989, pp. 281–288.
[9] Simon, V., EHD lubrication of double enveloping worm gears, in: Proceedings, Japan International Tribology Conference, Nagoya, 1990, pp. 1527–1532.
[10] V. Simon, Load distribution in double enveloping worm gears, ASME Journal of Mechanical Design 115 (1993) 496–501.
[11] H. Gunbara, S. Shimachi, T. Kobayashi, H. Kawada, A study on hourglass-worm gearings designed to concentrate surfaces normals: design for worm gearings with large lead angle, in: Proceedings of 6th International Power Transmission and Gearing Conference, Scottsdale, 1992, pp. 153–159.
[12] H.S. Fang, C.B. Tsay, Mathematical model and bearing contacts of the ZN-type worm gear sets cut by oversize hob cutters, Mechanism and Machine Theory 35 (12) (2000) 1689–1708.
[13] W.L. Janninck, Contact surface topology of worm gear teeth, Gear Technology (1988) 31–47.
[14] F.L. Litvin, Gear Geometry and Applied Theory, PTR Prentice Hall, New Jersey, 1994.
[15] F.L. Litvin, A. Fuentes, Gear Geometry and Applied Theory, second ed., Cambridge University Press, 2004.
[16] W. Shi, D. Qin, W. Xu, Meshing control of the double-enveloping worm gearing under the conditions of existing the errors and the load, Mechanism and Machine Theory 39 (2004) 61–74.